Engineering 9 (2022) 67–76

Contents lists available at ScienceDirect

Engineering

journal homepage: www.elsevier.com/locate/eng

Research
Advanced Water Science and Technology—Article

The Crystallization Behavior and Stability of Chromite Synthesized in Chromium-Containing Wastewater at Room Temperature

Jin-Fang Lv [a], Ying-Cong Quan [a], Xiong Tong [a,b], Yongjun Peng [c], Yong-Xing Zheng [b,*]

[a] Faculty of Land Resource Engineering, Kunming University of Science and Technology, Kunming 650093, China
[b] State Key Laboratory of Complex Nonferrous Metal Resources Clean Utilization, Kunming University of Science and Technology, Kunming 650093, China
[c] School of Chemical Engineering, The University of Queensland, Brisbane, QLD 4072, Australia

ARTICLE INFO

Article history:
Received 6 May 2020
Revised 27 August 2020
Accepted 12 September 2020
Available online 4 March 2021

Keywords:
Chromium-containing wastewater
Synthesis of chromite
Room temperature
Crystallization behavior
Stability

ABSTRACT

The ferrite process can not only purify wastewater containing heavy metal ions but also recycle valuable metals from wastewater. Therefore, it is considered a promising technology to treat chromium-containing wastewater. However, the process has not been extensively applied in industry due to its high synthesis temperature. In this paper, the feasibility of chromite synthesis at room temperature was comprehensively studied. The effects of critical factors on the effluent quality and the crystallization behavior and stability of the synthetic products were investigated. Results showed that the removal ratio of chromium from wastewater was over 99.0%, and the chromium concentration in the supernatant reached the sewage discharge standard after undergoing the ferrite process at room temperature. Increases in the aeration rate, stirring rate, and reaction time were favorable for the formation of stable chromite. The particles obtained by the ferrite process at room temperature were characterized by a compact structure, and the maximum size of the particles reached 52 μm. Chromium gradually entered the spinel crystal structure during the synthesis process, and the molecular formula of the synthetic chromite might be $Fe_{3-x}Cr_xO_4$, in which x was approximately 0.30. The path of the microscopic reaction was proposed to illuminate the synthesis mechanism of chromite under room temperature conditions. The present study has laid the foundation for the industrial application of the ferrite process in the purification and utilization of chromium-containing wastewater.

© 2021 THE AUTHORS. Published by Elsevier LTD on behalf of Chinese Academy of Engineering and Higher Education Press Limited Company. This is an open access article under the CC BY-NC-ND license (http://creativecommons.org/licenses/by-nc-nd/4.0/).

1. Introduction

Ores and compounds containing chromium are widely applied in industrial manufacturing, such as metallurgy, electroplating, and tannery [1–3]. However, chromium is a considerably toxic inorganic contaminant and easily enters water and soil during production [4–6]. Cr(VI) and Cr(III) are the main states observed in the natural environment, and the toxicity of Cr(VI) is 100 times greater than that of Cr(III) [7]. Therefore, the reduction of Cr(VI) into Cr(III) has been a hot research topic for the purification of chromium-containing wastewater. The reduction methods mainly include chemical reduction [8–10], photocatalytic reduction [11–13], and bioremediation [14–16]. At present, chemical reduction has become a universal commercial method due to its easy operation and use of inexpensive chemicals [17,18]. However, an abundance of toxic sludge, which is classified as hazardous waste [19], is generated during chemical reduction. The plants that produce this sludge have to pay considerable amounts of money to professional institutions that treat sludge, which usually choose to fill or solidify the waste. Moreover, considerable amounts of valuable metals existing in the sludge are lost, and the risk of secondary contamination is present. Therefore, it is necessary to explore an alternative technique that can not only purify chromium-containing wastewater but also recycle valuable metals in the wastewater [20].

The ferrite process, which can synthetize spinel minerals with stable structures and magnetic properties, has received extensive attention in the treatment of chromium-containing wastewater [21–24]. The chromium in wastewater can not only be removed but also be converted into stable chromite, which is viewed as a resource (Eqs. (1)–(4)) [25,26]. Thus, the secondary pollution of chromium in the environment will be avoided, and the obtained

* Corresponding author.
E-mail address: yongxingzheng2017@126.com (Y.-X. Zheng).

https://doi.org/10.1016/j.eng.2020.12.018
2095-8099/© 2021 THE AUTHORS. Published by Elsevier LTD on behalf of Chinese Academy of Engineering and Higher Education Press Limited Company.
This is an open access article under the CC BY-NC-ND license (http://creativecommons.org/licenses/by-nc-nd/4.0/).

chromite will be perfectly utilized. Erdem and Tumen [21] confirmed that Cr(III) in aqueous solution could be completely removed and that the synthetic product was stable chromite through the use of the ferrite process at 50 °C. Pei et al. [22] investigated chromium-containing wastewater with an initial chromium concentration of 1539 mg·L^{-1} and used the ferrite process at 75 °C. The results showed that the removal ratio of chromium reached 99.97%. Furthermore, the ferrite process was also effective in the purification of polymetallic wastewater containing chromium. Song et al. [23] reported the treatment of wastewater containing chromium and nickel ions by the ferrite process at 70 °C. The results indicated that the removal ratios of chromium and nickel ions were approximately 98% and that the synthetic Ni–Cr ferrite had good chemical stability. Tu et al. [24] adopted multiple stages of ferrite processes above 70 °C to treat wastewater containing Cr, Cd, Cu, and Pb. The results showed that the concentrations of heavy metals in the supernatant reached the discharge standards and that the formed sludge exhibited stable chemical properties.

$$Cr^{3+} + 3OH^- \rightarrow Cr(OH)_3 \quad (1)$$

$$Fe^{2+} + 2OH^- \rightarrow Fe(OH)_2 \quad (2)$$

$$Fe^{3+} + 3OH^- \rightarrow Fe(OH)_3 \quad (3)$$

$$Fe^{2+} + 2Cr^{3+} + 8OH^- \rightarrow FeCr_2O_4 + 4H_2O \quad (4)$$

Previous studies have shown that the removal ratio of chromium can reach above 90%. Moreover, the effluent quality and stability of synthetic products can meet standards after treatment by the ferrite process. However, the reaction temperature usually needs to be kept above 70 °C to improve the crystal growth of the synthetic products [24,27]. This high temperature restricts the further industrial application of the ferrite process due to the high cost and difficult operation. The high reaction temperature requires consuming large amounts of coal to provide thermal energy. Additionally, many organic pollutants existing in the chromium-containing wastewater will readily evaporate into the air, causing serious air pollution. To solve these problems, it is particularly important to synthesize chromite at lower temperatures, even reaching room temperature.

In the present study, the feasibility of chromite synthesis in chromium-containing wastewater at room temperature was investigated and the crystallinity and stability of the synthetic products were improved by optimizing the reaction parameters. The effects of temperature, initial pH, dose of ferrous sulfate, aeration rate, stirring rate, and reaction time on the crystallization behavior and stability of synthetic chromite were examined by atomic absorption spectrophotometry (AAS), X-ray diffraction (XRD), and leaching toxicity tests. The surface morphology and composition of synthetic chromite were detected by scanning electron microscopy (SEM) and energy dispersive spectroscopy (EDS), respectively. It was believed that the study will provide a theoretical reference to facilitate the industrial application of the ferrite process for treating chromium-containing wastewater at room temperature.

2. Materials and methods

2.1. Materials

Cr(VI) was the major valence state of chromium in the electroplating wastewater. It was initially reduced to Cr(III) by reducing reagents, and then ferrous ions were added to synthesize chromite. Therefore, chromium sulfate ($Cr_2(SO_4)_3·6H_2O$) was chosen as the object of study. Chromium sulfate, ferrous sulfate, and other chemical reagents used in this study were of analytical reagent (AR) grade. To prepare a 100 mg·L^{-1} Cr(III) aqueous solution, 0.144 g of chromium sulfate was added into a 500 mL beaker loaded with 300 mL of deionized water. Compressed air with an oxygen concentration of 21% was used as an oxidant in the experiments.

2.2. Experimental methods

Fig. 1 shows the schematic diagram of the experimental apparatus. Ferrous sulfate was homogeneously mixed with a solution containing 100 mg·L^{-1} Cr(III). Then, the pH of the mixed solution was rapidly adjusted to the required value by sulfuric acid or sodium hydroxide. After that, the solution was placed into a 500 mL three-necked flask. Compressed air was introduced at a particular flow rate, and the solution was simultaneously stirred by mechanical agitation. When the desired reaction time was reached, solid–liquid separations were carried out in a filter flask, and the solid residue and supernatant were obtained. The solid products were analyzed by XRD, SEM–EDS, and leaching toxicity tests. The supernatant was used to test the concentrations of chromium and iron ions by AAS.

2.3. Analytical techniques

The phases of the synthetic products were detected by an X-ray diffractometer (Rigaku D/Max 2200, Japan). The surface morphology and composition of the synthetic products were examined by SEM (FEI Quanta 600, the Netherlands) and EDS (EDAX Apollo X, USA). The magnetic properties of the synthetic products were tested by a vibrating sample magnetometer (Zetian BKT-4500,

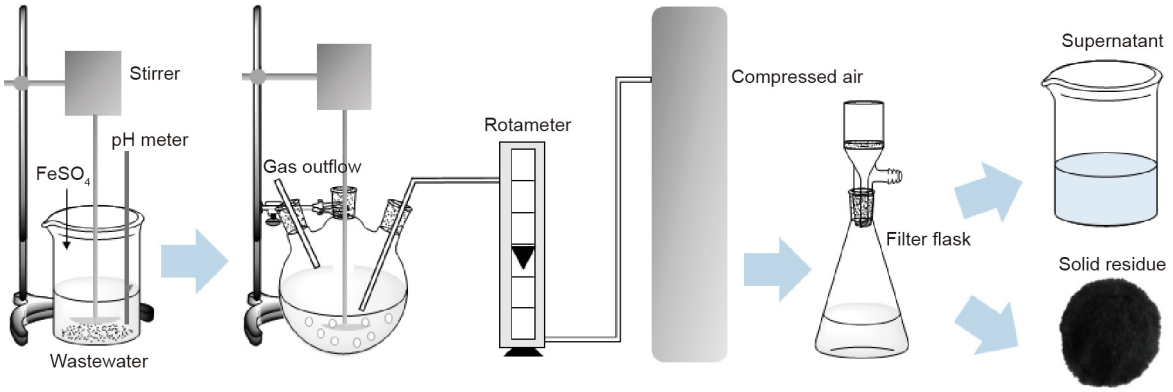

Fig. 1. Schematic diagram of the experimental apparatus.

China). The remaining concentrations of chromium and iron ions in the supernatant were analyzed by atomic absorption spectrophotometry (Rayleigh WFX-320, China). The oxidation–reduction potential (ORP) and pH were monitored by a potential–pH meter (Leici PHS-3C, China). The proposed path diagram of the microscopic reaction was drawn in MedeA v3.1 software.

According to the solid waste-extraction procedure for leaching toxicity in China, leaching toxicity tests were conducted [28–30]. Sulfuric acid and nitric acid were initially mixed at a molar ratio of 2:1. The mixture was added into distilled water to adjust the pH to 3.2, and the resulting solution was used as the leaching reagent. Then, the synthetic products were placed into the leaching reagent at a ratio of 1:10 (kg·L^{-1}), and horizontal vibration (110 rotations per minute (rpm)) was applied. After reacting for 8 h, the solution was allowed to stand for 16 h. Finally, the solution was filtered in a filter flask, and the concentration of chromium ions in the supernatant was analyzed by AAS.

3. Results and discussion

3.1. Effect of temperature

The reaction temperature usually plays a crucial role in the synthesis of ferrite [31–33]. To investigate the effects of temperature on the removal ratios of chromium and iron ions from chromium-containing wastewater, experiments were carried out, and the results are shown in Fig. 2. The removal ratios of chromium and iron ions slightly fluctuated in the given temperature range, which indicated that the effects of temperature on their removal ratios were not significant. The residual concentration of chromium in the solution after the reaction was below 0.60 mg·L^{-1}, corresponding to a chromium-ion removal ratio above 99.0%. According to the standard of sewage discharge in China [34], the concentration of total chromium ions in the solution was below 1.50 mg·L^{-1}. Therefore, the residual concentration of chromium ions in the solution after the treatment reached the standard. In addition, the remaining concentration of iron ions in the solution after the treatment was less than 55.0 mg·L^{-1}, corresponding to a removal ratio of iron ions above 98.5%.

Fig. 3 shows the XRD patterns of the synthetic products at different temperatures. It can be observed that the peak intensity of the synthetic products was enhanced with increasing reaction temperature, indicating that a higher temperature was conducive to the crystallization of products. It could be explained that the increase in reaction temperature accelerated the hydrolysis and dehydration reactions of the ferrite precursor [35]. However, weak characteristic peaks of the synthetic products also occurred when the reaction was fixed at room temperature. Considering its practical operation and low cost, room temperature was initially selected for the following experiments.

Toxicity leaching tests were further conducted to investigate the stability of the synthetic products at different temperatures, as shown in Fig. 4. The concentration of chromium in the leaching solution was lower than 5.0 mg·L^{-1} at different temperatures, which reached the US Environmental Protection Agency (US EPA) toxic leaching limit [21]. These results indicated that the chromite synthesized at room temperature was stable. Therefore, it was feasible to synthesize chromite at 25 °C.

3.2. Effect of initial pH

Based on previous studies, the formation of chromite in wastewater initially required the coprecipitation of Cr(III), Fe(II), and Fe(III) (Eqs. (1)–(4)). Nevertheless, excessive OH^- would cause these precipitates, such as $Cr(OH)_3$, $Fe(OH)_2$, and $Fe(OH)_3$, to dissolve again [36–38]. Therefore, the initial pH of the aqueous

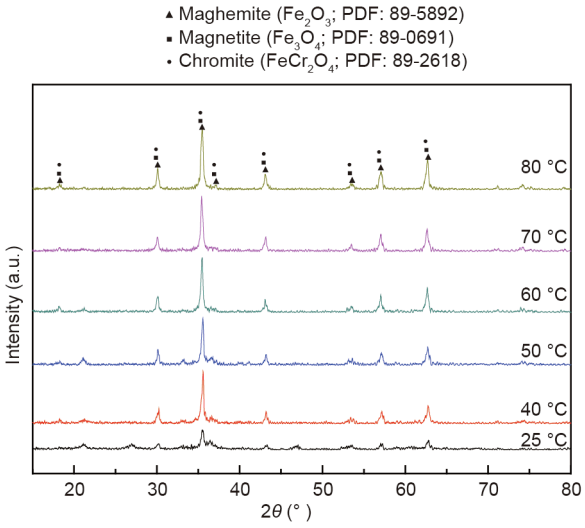

Fig. 3. XRD patterns of the synthetic products at different temperatures. a.u.: arbitrary unit; PDF: powder diffraction file; 2θ: scattering angle.

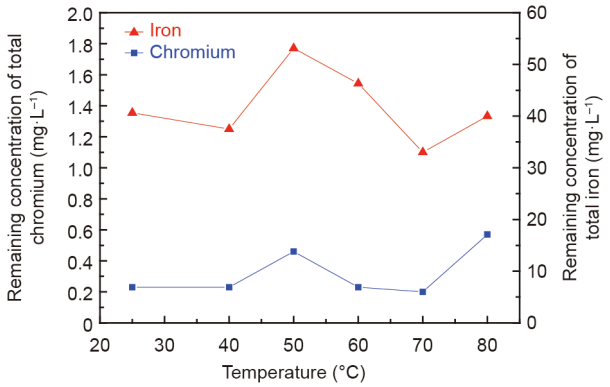

Fig. 2. Effects of reaction temperatures on the concentrations of total chromium and iron ions in the supernatant after the reaction (C_0 (initial concentration of Cr(III)): 100 mg·L^{-1}; molar ratio of Fe(II) and Cr(III): 8:1; initial pH: 9.5; stirring rate: 300 rotations per minute (rpm); aeration rate: 200 mL·min^{-1}; reaction time: 60 min).

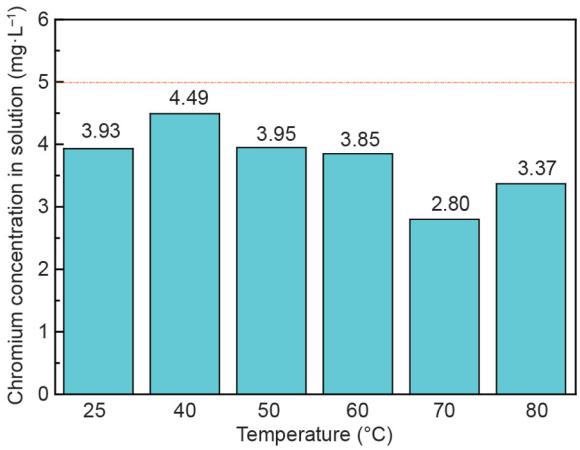

Fig. 4. Results of the leaching toxicity of the synthetic products at different temperatures.

solution was selected to be in the range of 8.5–11.5 in this study. Figs. 5 and 6 show the effects of the initial pH on the effluent quality and crystallization behavior of the synthetic products, respectively. From Fig. 5, the chromium concentration in the supernatant after chromite synthesis decreased to below 0.25 mg·L^{-1} in the presented pH range, corresponding to chromium removal ratios greater than 99.5%. These results indicated the outstanding removal performance of chromium ions.

In addition, the remaining concentrations of total iron in the supernatant after synthesis rapidly decreased from 68.6 to 4.7 mg·L^{-1} when the initial pH value increased from 8.5 to 10.5. Correspondingly, the removal ratio of iron ions increased to above 98%. With a further increase in the initial pH value, the remaining concentrations of total iron slightly decreased. These results confirmed that the increase in initial pH was beneficial to the removal of iron ions from the wastewater.

From Fig. 6, it is observed that lepidocrocite was the only synthetic product when the initial pH of the solution was fixed at 8.5, which suggested that it was unbeneficial to synthesize chromite at lower pH values. When the initial pH of the solution increased to 9.5, the peak intensity of lepidocrocite decreased, while the characteristic peaks of chromite began to appear [22,39]. However, it also seemed to be possible that the peak signals represented magnetite or maghemite due to their extraordinarily similar locations with chromite. When the initial pH of the solution increased to 10.5, only the characteristic peaks of chromite were observed. With a further increase in the initial pH of the solution to 11.5, the peak intensity of chromite clearly decreased, suggesting that having a solution at higher pH values was not beneficial for the crystallization of chromite. However, it seemed to be contradictory in contrast with the results obtained in Fig. 5, in which the removal performances of chromium and iron ions were excellent. This result may be accounted for by the fact that the generated polyhydric ions, such as $Cr(OH)_4^-$, $Fe(OH)_3^-$ and $Fe(OH)_4^-$, might adsorb on the solid surface [37,40]. Therefore, the optimum pH for synthesizing chromite was determined to be within the scope of 9.5–10.5 at room temperature, and this pH range was nearly consistent with that of previous studies [22,24,25].

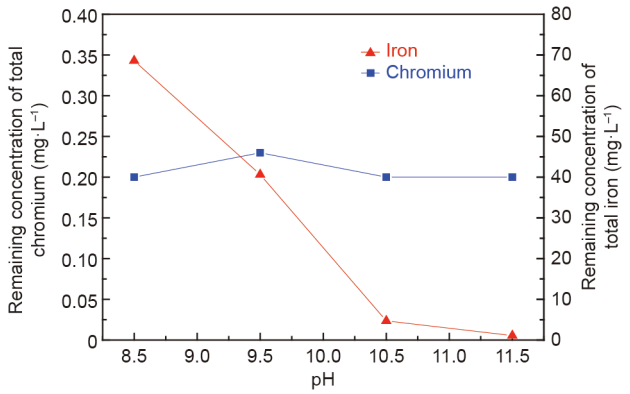

Fig. 5. Effects of the initial pH on the remaining concentrations of the total chromium and iron ions in the supernatant after reaction (C_0: 100 mg·L^{-1}; molar ratios of Fe(II) and Cr(III): 8:1; aeration rate: 200 mL·min^{-1}; stirring rate: 300 rpm; room temperature; reaction time: 60 min).

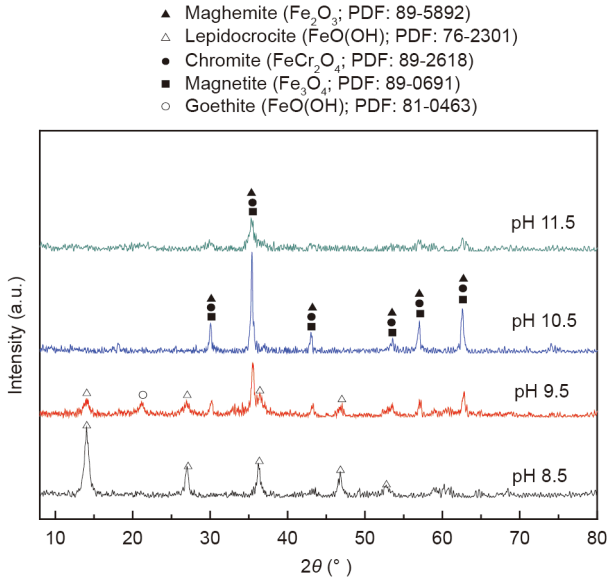

Fig. 6. XRD patterns of the synthetic products at different initial pH values.

To gain insight into the synthesis process of chromite, the ORP (E) and pH of the solution were detected, and the E–pH diagram of the Cr–Fe–H_2O system at room temperature was plotted, as shown in Fig. 7. Fig. 7(a) shows that the pH of the solution gradually decreased from 9.60 to 4.96 as the reaction time increased. However, the ORP gradually increased from −0.278 to 0.315 V as the reaction time increased. Combined with the E–pH diagram (Fig. 7(b)), the main area consisted of chromite when the pH was varied in the range of 4.96–9.60, and the potential was within the range of −0.278 to 0.315 V. Therefore, chromite was efficiently synthesized at room temperature after the other parameters were optimized.

3.3. Effect of the ferrous sulfate dose

The effects of the ferrous sulfate dose on the effluent quality were investigated, as shown in Fig. 8. The remaining concentrations of total chromium after the synthesis were below 0.23 mg·L^{-1} in the range of the presented Fe(II)/Cr(III) mole ratios, and the concentration met the sewage discharge standards in China [34]. Correspondingly, the removal ratios of chromium reached above 99.0%, indicating that chromium ions underwent hydroxide precipitation or oxide precipitation. Moreover, the remaining concentrations of total iron increased from 1.40 to 40.61 mg·L^{-1} when the Fe(II)/Cr(III) mole ratio increased from 2.0 to 8.0, which was attributed to the addition of more ferrous sulfate. The removal ratio of iron ions also reached above 99.0%.

Fig. 9 shows the XRD patterns of the synthetic products obtained at different Fe(II)/Cr(III) molar ratios. There were no diffraction peaks when the initial Fe(II)/Cr(III) mole ratio was 1:1, which indicated that there were no products to be synthesized or that the synthetic products were amorphous compounds. This result may be accounted for by the formation of $Fe(OH)_2$, $Fe(OH)_3$, and $Cr(OH)_3$ (Eqs. (1)–(3)) [25,26]. The peak signals of chromite started to occur when the initial Fe(II)/Cr(III) molar ratio increased to 4:1. With a further increase in the initial Fe(II)/Cr(III) molar ratio to 8:1, the peak intensity of chromite was clearly enhanced, indicating that chromite with good crystallization was formed.

3.4. Effect of the aeration rate

To investigate the effects of the aeration rate on the effluent quality, a batch of experiments were carried out, and the results are shown in Fig. 10. The concentrations of chromium and iron ions in the solution were less than 0.23 and 40.0 mg·L^{-1}, respectively.

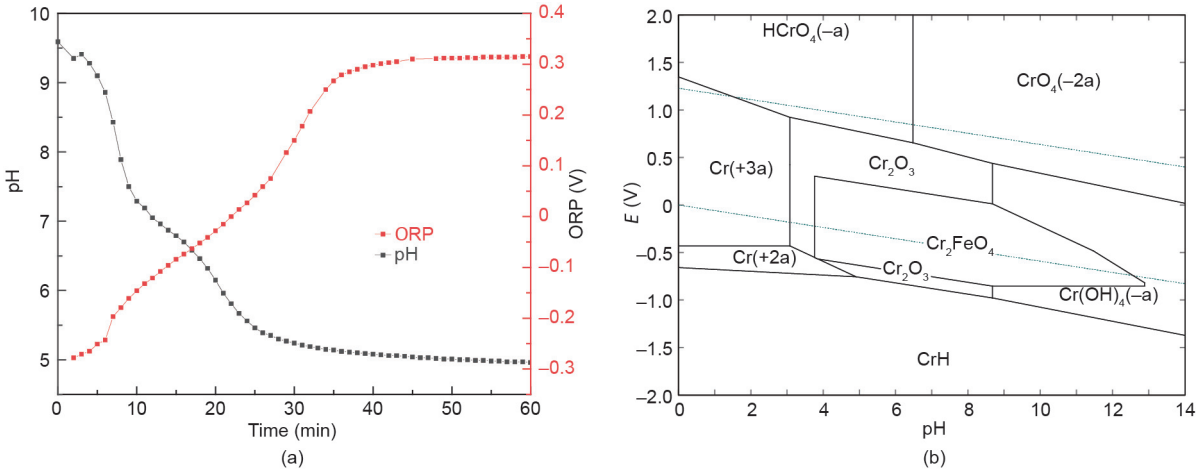

Fig. 7. (a) Variation in the pH and ORP during the experiment at an initial pH of 9.5, and (b) the *E*–pH diagram of the Cr–Fe–H_2O system at room temperature (−a: aqueous species with a negative valence; −2a: aqueous species with two negative valences; +2a: aqueous species with two positive valences; +3a: aqueous species with three positive valences).

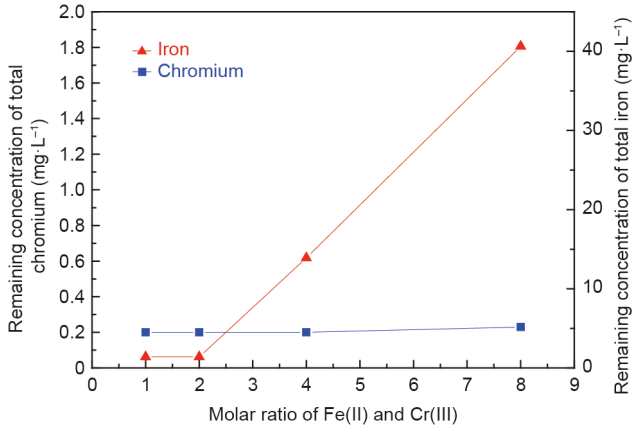

Fig. 8. Effects of various molar ratios of Fe(II) and Cr(III) on the remaining concentrations of chromium and iron ions in the supernatant after the reaction (C_0: 100 mg·L^{-1}; initial pH: 9.5; aeration rate: 200 mL·min^{-1}; stirring rate: 300 rpm; room temperature; reaction time: 60 min).

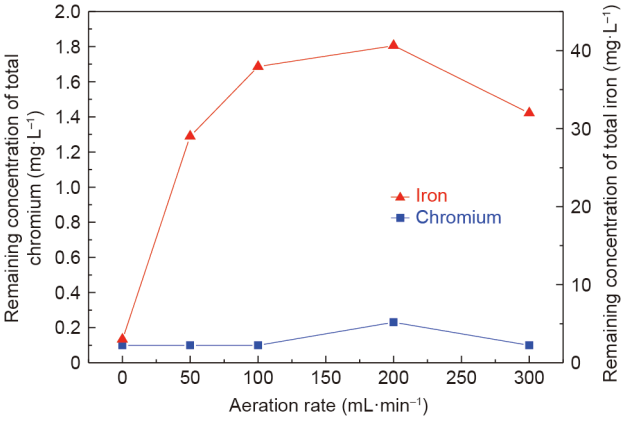

Fig. 10. Effects of the aeration rate on the remaining concentrations of total chromium and iron ions in the supernatant after the reaction (C_0: 100 mg·L^{-1}; molar ratio of Fe(II) and Cr(III): 8:1; initial pH: 9.5; stirring rate: 300 rpm; room temperature; reaction time: 60 min).

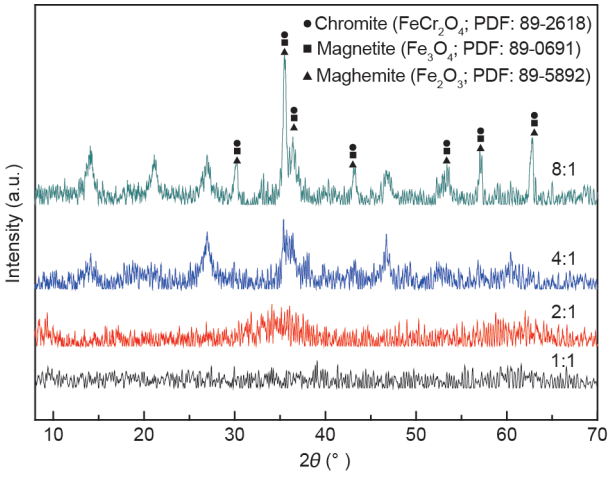

Fig. 9. XRD patterns of the synthetic products at different molar ratios of Fe(II) and Cr(III).

The removal ratios of chromium and iron ions were above 99.0%, thereby reaching the emission standard.

To ascertain the effects of the aeration rate on the crystallization behavior and stability of synthetic products, XRD and leaching toxicity tests were performed, and the results are shown in Figs. 11 and 12. From Fig. 11, the peak intensity of chromite increased when the aeration rate increased from 50 to 100 mL·min^{-1}. When the aeration rate increased to 200 mL·min^{-1} and even 300 mL·min^{-1}, the peak intensity of the chromite continuously decreased. This result can be explained by the fact that the increase in aeration rate accelerated the formation of chromite nuclei while inhibiting the growth of crystal nuclei. In addition, it is observed that the peaks of the synthetic products shifted toward high diffraction angle areas with an increasing aeration rate, which indicated that chromite with a higher chromium content was synthesized. This result was accounted for by the fact that Cr(III) with a radius of 0.63 Å gradually substituted Fe(III) with a radius of 0.67 Å in the spinel structure, thereby resulting in the continuous contraction of the unit cell [41].

According to Fig. 12, the chromium concentration in the leaching solution was 9.58 mg·L^{-1}, which was above 5 mg·L^{-1} for the

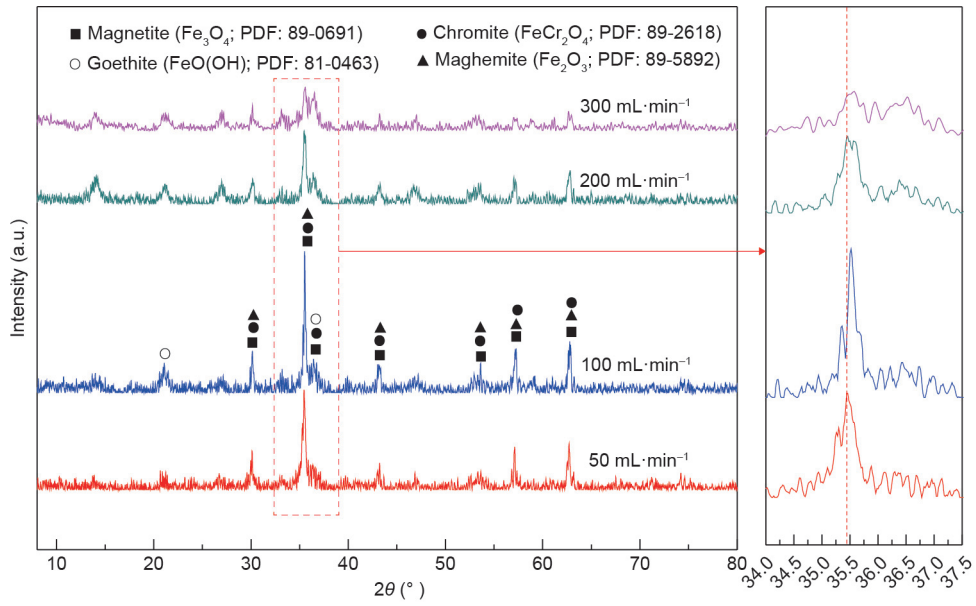

Fig. 11. XRD patterns of the synthetic products at different aeration rates.

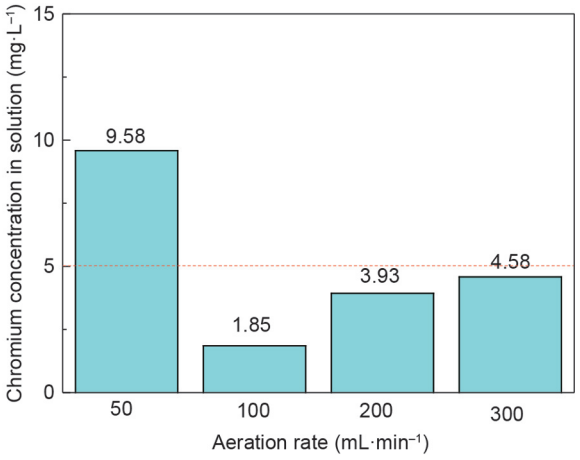

Fig. 12. Leaching toxicity results of the synthetic products at different aeration rates.

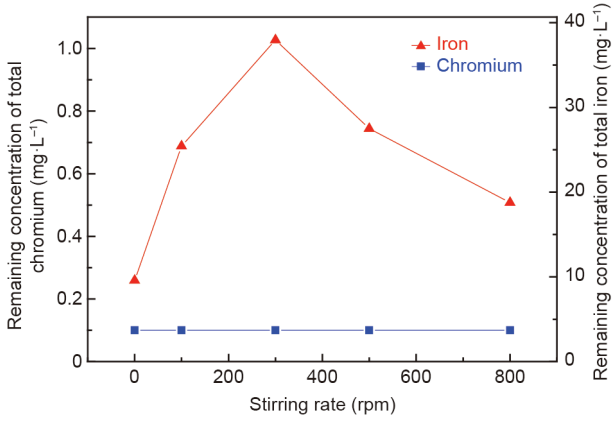

Fig. 13. Effects of the stirring rate on the remaining concentrations of total chromium and iron ions in the supernatant after the reaction (C_0: 100 mg·L^{-1}; molar ratio of Fe(II) and Cr(III): 8:1; initial pH: 9.5; aeration rate: 100 mL·min^{-1}; room temperature; reaction time: 60 min).

standard issued by the US EPA [21], when the aeration rate was fixed at 50 mL·min^{-1}. When the aeration rate was increased to 100 mL·min^{-1}, the chromium concentration in the leaching solution decreased to 1.85 mg·L^{-1}. With a further increase in the aeration rate, the chromium concentration in the leaching solution gradually increased, but the chromium concentration was less than the standard. Lower or higher aeration rates were not favorable for the stability of chromite synthesized in wastewater. These results might be accounted for by the fact that too few or too many ferrous ions were transformed into trivalent iron, resulting in an imbalance between ferrous and ferric ions to form a spinel structure [35].

3.5. Effect of the stirring rate

To investigate the effects of the stirring rate on effluent quality, a batch of experiments were carried out, and the results are shown in Fig. 13. The remaining concentrations of chromium and iron ions in solution were 0.1 and less than 38.0 mg·L^{-1}, respectively, corresponding to removal ratios of above 99.0% for both chromium and iron ions, and these values reached the emission standard.

The effects of the stirring rate on the crystallization behavior and stability of the synthetic products were also investigated. The XRD and leaching toxicity test results are presented in Figs. 14 and 15, respectively. From Fig. 14, the peak signals of chromite were obvious when the stirring rates were within the scope of 0 to 500 rpm. When the stirring rate was increased to 800 rpm, the peak signal nearly disappeared. Moreover, when the stirring rate increased from 300 to 500 rpm, the peaks of the synthetic products shifted toward a high diffraction angle area, which was explained by the fact that more Cr(III) with a radius of 0.63 Å substituted Fe(III) with a radius of 0.67 Å in the spinel structure and resulted in the continuous contraction of the unit cell [41]. Therefore, chromite with a higher chromium content was synthesized. According to Fig. 15, the chromium concentrations in the leaching solution decreased from 46.60 to 1.85 mg·L^{-1} when the stirring rates increased from 0 to 300 rpm. Combined with the XRD results, chromite could be generated at lower stirring rates (0–100 rpm), but Cr(III) seemed to not completely enter the stable spinel

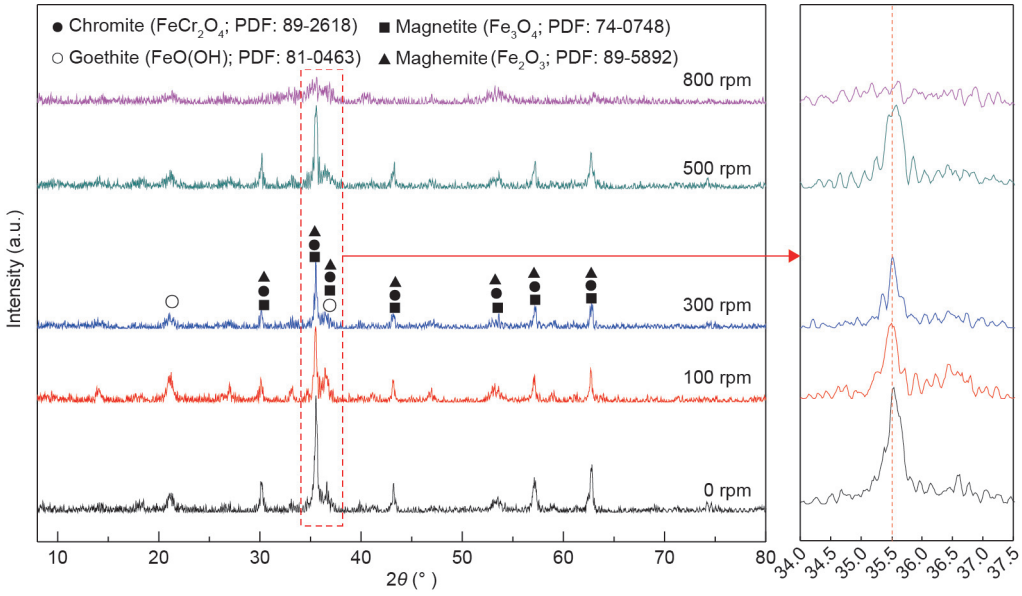

Fig. 14. XRD patterns of the synthetic products at different stirring rates.

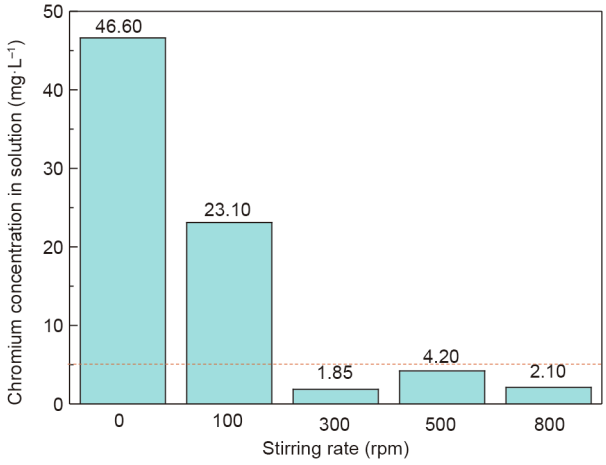

Fig. 15. Leaching toxicity results of the synthetic products at different stirring rates.

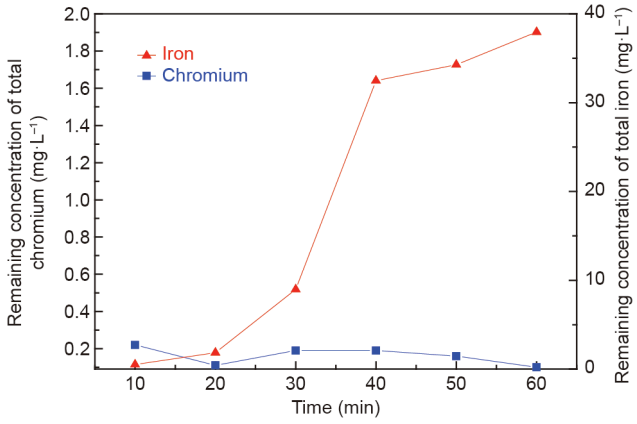

Fig. 16. Effects of the reaction time on the remaining concentrations of total chromium and iron ions in the supernatant after the reaction (C_0: 100 mg·L^{-1}; molar ratio of Fe(II) and Cr(III): 8:1; initial pH: 9.5; stirring rate: 300 rpm; aeration rate: 100 mL·min^{-1}; room temperature).

structure, which may be explained by the fact that the solution had a lower rate of mass transfer for Cr(III).

3.6. Effect of the reaction time

To investigate the effects of the reaction time on effluent quality, a batch of experiments were carried out, and the results are shown in Fig. 16. The remaining concentrations of chromium and iron ions in the solution were less than 0.22 and 37.95 mg·L^{-1}, respectively, which corresponded to the removal ratios of both chromium and iron ions to be above 99.0%.

The effects of reaction time on the crystallization behavior and stability of the synthetic products were examined. The XRD and leaching toxicity test results are shown in Figs. 17 and 18, respectively. According to Fig. 17, the peak signals of chromite were obvious when the reaction time was fixed at 30 and 40 min. With a further increase in the reaction time, the peak intensity of chromite increased. Additionally, the peaks of the synthetic products shifted toward high diffraction angle areas with an increasing reaction time, which suggested that chromite with a high chromium content was synthesized. From Fig. 18, the chromium concentration in the leaching solution continuously decreased with increasing reaction time. When the reaction time was fixed at 60 min, the chromium concentration in the leaching solution decreased to 1.85 mg·L^{-1}, which was less than the standard. These results further confirmed that chromite with a low chromium content evolved into chromite with a high chromium content.

3.7. Morphology and magnetic properties of the synthetic products

To further interpret the morphology and magnetic properties of the synthetic products, morphology and magnetic hysteresis loop analyses were carried out, and the results are shown in Fig. 19. Fig. 19(a) shows that the synthetized particles with rough surfaces had compact structures. In addition, the particles exhibited irregular hexahedral characteristics. The maximum size of the obtained particles reached 52 μm. The magnetic hysteresis loops of the synthetic products, as presented in Fig. 19(b), show that the remanence and coercive force of the synthetic products were very small. In other words, the hysteresis loop was narrow, suggesting that the synthetic products were soft magnetic materials. On the

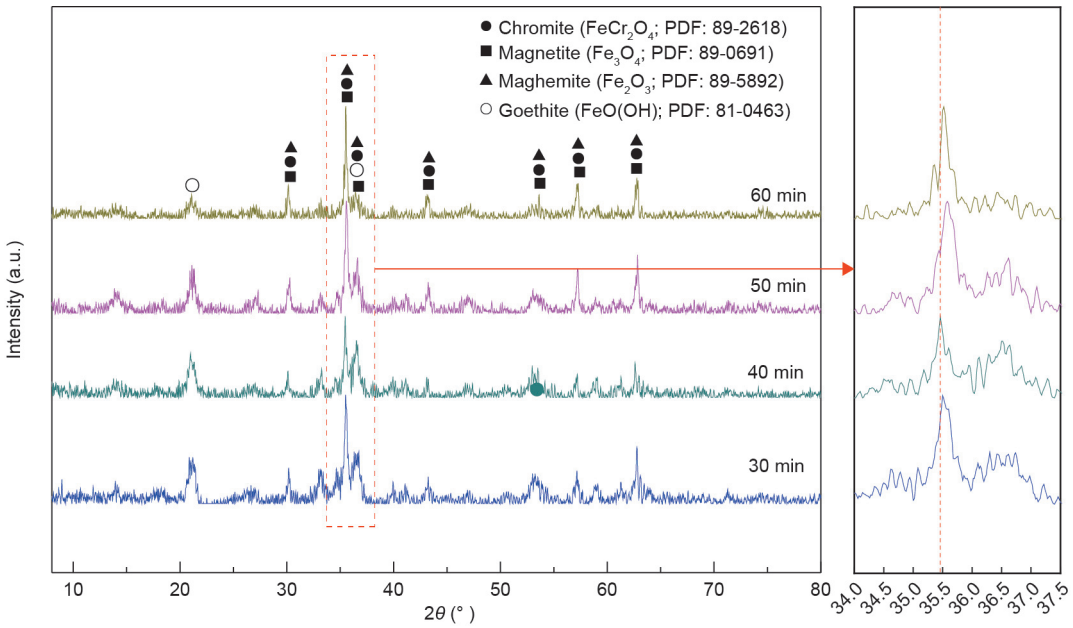

Fig. 17. XRD patterns of the synthetic products at different reaction times.

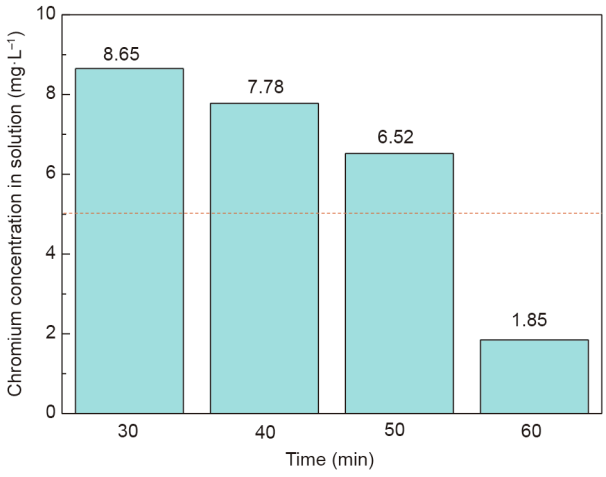

Fig. 18. Leaching toxicity results of the synthetic products at different reaction times.

other hand, the saturation magnetization of the synthetic products reached 1.6 emu·g^{-1} (1 emu·g^{-1} = 1 A·m^2·kg^{-1}). These results indicated that the synthetic products could be recovered in the following separation.

3.8. Path of the microscopic reaction

To reveal the migration rule of the chromium ions in the process of chromite synthesis in wastewater at room temperature, the synthesized minerals were further analyzed by SEM–EDS, and the results are shown in Fig. 20. Fig. 20(a) shows that the color was different between the center and the edge of the synthetic minerals. Combined with the EDS results (Figs. 20(b) and (c)), it was confirmed that the content of chromium in the center was higher than that at the edge of the synthetic minerals. This result implied that chromium gradually entered the synthetic chromite structure as the reaction proceeded, which agreed with the conclusions obtained in Section 3.6. From Figs. 20(d)–(f), it is observed that the distribution of Fe, Cr, and O in the synthetic minerals

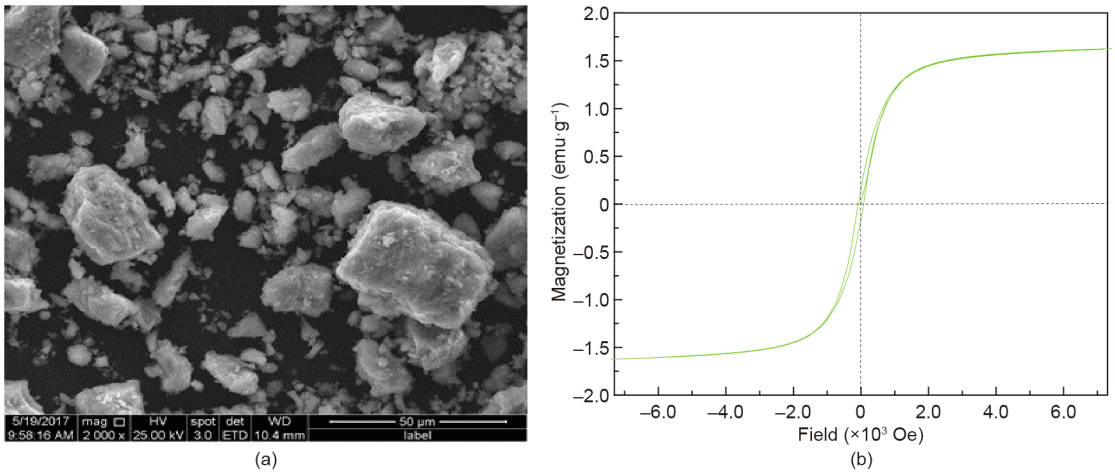

Fig. 19. (a) Morphology and (b) magnetic hysteresis loops of the synthetic products. 1 emu·g^{-1} = 1 A·m^2·kg^{-1}; 1 Oe = $10^3/(4\pi)$ A·m^{-1}.

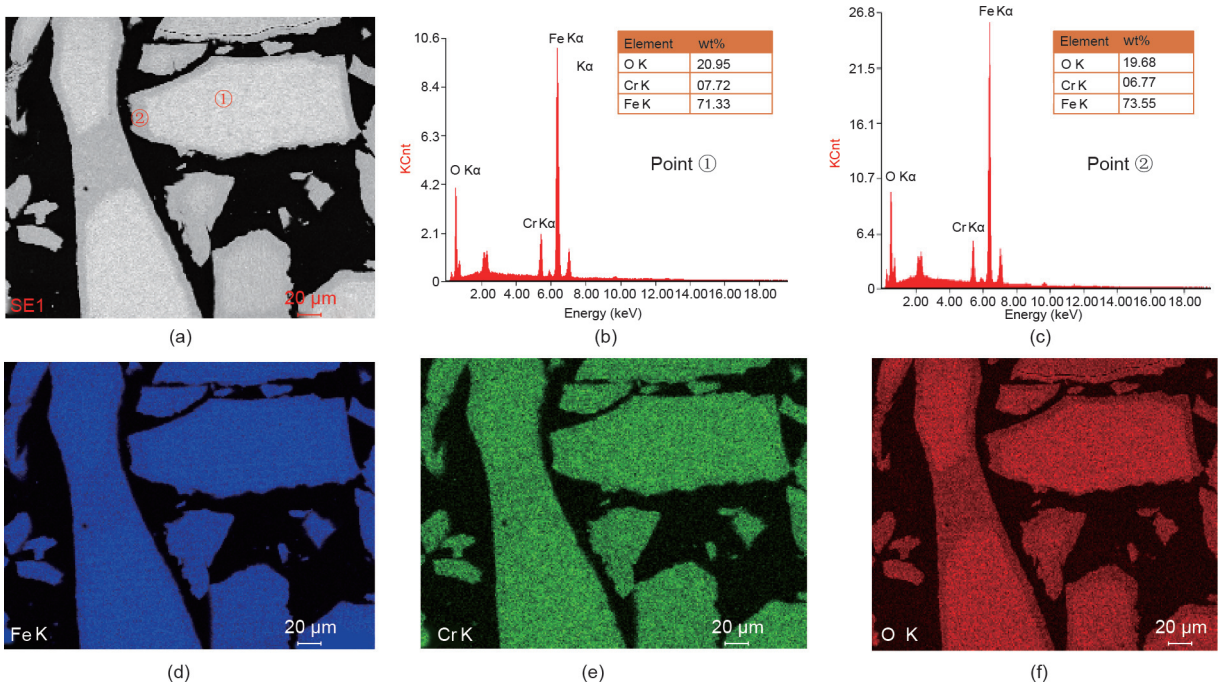

Fig. 20. SEM–EDS results of the synthetic products: (a) SEM image; (b, c) EDS at a specific position; and (d)–(f) Fe, Cr, and O distribution images. KCnt: 1000 counts; Kα: X-rays radiated by transition from shell L to shell K.

overlapped, which indicated that the synthesized minerals might be single chromite. Combined with the EDS results (Figs. 20(b) and (c)), it was further calculated that the molecular formula of the synthetic chromite might be $Fe_{3-x}Cr_xO_4$, where x was approximately 0.30.

Based on the above results, the path of the microscopic reaction was proposed, and the results are shown in Fig. 21. According to the figure, a small amount of chromium ions preferentially entered the spinel structure at the beginning of the synthetic reaction, leading to the formation of stable chromite with a low chromium content. Moreover, the remaining chromium ions formed chromium hydroxide or unstable chromite. As the reaction continued, more chromium ions entered the unit cell of chromite and formed stable chromite with a high chromium content. In other words, the concentrations of chromium ions in the unit cell gradually increased during the synthesis of chromite. Finally, approximately all the chromium ions entered the chromite with the following chemical formula, $Fe_{3-x}Cr_xO_4$. The x value in $Fe_{3-x}Cr_xO_4$ was far lower than the theoretical value in $FeCr_2O_4$, which could be explained by the fact that the concentrations of chromium ions were far less than those of ferrous ions at the beginning of the synthesis process.

4. Conclusions

The present study demonstrated the feasibility of chromite synthesis in chromium-containing wastewater by the ferrite process at room temperature. Some conclusions are summarized below.

(1) After treating chromium-containing wastewater by the ferrite process, a chromium removal ratio of more than 99.0% from the supernatant was obtained, and the chromium concentrations reached the sewage discharge standard. The optimum process parameters were determined as follows: initial pH range: 9.5–10.5; initial Fe(II)/Cr(III) molar ratio: 8:1; aeration rate: 100 mL·min^{-1}; stirring rate: 300 rpm; and reaction time: 60 min. Under these conditions, the chromium concentration in the solution reached 1.85 mg·L^{-1} after leaching the synthetic products.

(2) The parameters, such as temperature, pH, ferrous sulfate dose, aeration rate, stirring rate, and reaction time, had obvious effects on the synthesis of chromite. Increasing these parameters were favorable for the crystallization and stability of chromite, but a higher pH, aeration rate, and stirring rate were not beneficial for the crystallization growth of chromite.

(3) Under room temperature conditions, the synthetized particles with rough surfaces had compact structures and exhibited

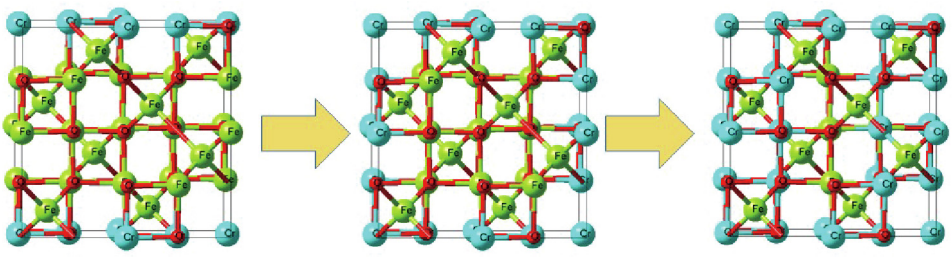

Fig. 21. Diagram of the proposed microscopic reaction path for chromite synthesis in wastewater at room temperature.

irregular hexahedral characteristics. The maximum size of the obtained particles reached 52 μm. The molecular formula of the synthetic products might be $Fe_{3-x}Cr_xO_4$, in which x was approximately 0.30. Finally, a microscopic reaction path was proposed for chromite synthesized in chromium-containing wastewater by the ferrite process at room temperature.

Acknowledgments

The authors would like to acknowledge the National Natural Science Foundation of China (51904129), the Basic Research Project of Yunnan Province (202001AU070028), and the Foundation of Yunnan's Education Ministry, China (2019J0037) for financial support.

Compliance with ethics guidelines

Jin-Fang Lv, Ying-Cong Quan, Xiong Tong, Yongjun Peng, and Yong-Xing Zheng declare that they have no conflict of interest or financial conflicts to disclose.

References

[1] Hemambika B, Kannan VR. Intrinsic characteristics of Cr^{6+}-resistant bacteria isolated from an electroplating industry polluted soils for plant growth-promoting activities. Appl Biochem Biotechnol 2012;167(6):1653–67.
[2] Lv JF, Zhang HP, Tong X, Fan CL, Yang WT, Zheng YX. Innovative methodology for recovering titanium and chromium from a raw ilmenite concentrate by magnetic separation after modifying magnetic properties. J Hazard Mater 2017;325:251–60.
[3] Hashem MA, Momen MA, Hasan M, Nur-A-Tomal MS, Sheikh MH. Chromium removal from tannery wastewater using *Syzygium cumini* bark adsorbent. Int J Environ Sci Technol 2019;16(3):1395–404.
[4] Lytras G, Lytras C, Argyropoulou D, Dimopoulos N, Malavetas G, Lyberatos G. A novel two-phase bioreactor for microbial hexavalent chromium removal from wastewater. J Hazard Mater 2017;336:41–51.
[5] Louarrat M, Rahman AN, Bacaoui A, Yaacoubi A. Removal of chromium Cr(VI) of tanning effluent with activated carbon from tannery solid wastes. Am J of Phys Chem 2017;6(6):103–9.
[6] Ateeq M, Rehman HU, Kiani BH, Zareen S, Maqbool T, Ilyas BS, et al. Toxic effect of hexavalent chromium on the workers employed in chrome plating. J Entomol Zool Stud 2017;5(1):221–3.
[7] Lu X, Li B, Guo L, Zhang G, Wang P. Reduction and stabilization remediation of hexavalent chromium (Cr^{6+})-contaminated soil. Ekoloji 2019;28(107):973–80.
[8] Xie B, Shan C, Xu Z, Li X, Zhang X, Chen J, et al. One-step removal of Cr(VI) at alkaline pH by UV/sulfite process: reduction to Cr(III) and *in situ* Cr(III) precipitation. Chem Eng J 2017;308:791–7.
[9] Lv J, Tong X, Zheng Y, Xie X, Huang L. Reduction of Cr(VI) with a relative high concentration using different kinds of zero-valent iron powders: focusing on effect of carbon content and structure on reducibility. J Cent South Univ 2018;25(9):2119–30. Chinese.
[10] Lv J, Tong X, Zheng Y. Removal behavior of Cu(II) during Cr(VI) reduction by cast iron powder in absence and presence of ultrasound. Sep Sci Technol 2019;54(18):3164–73.
[11] Zhao Z, An H, Lin J, Feng M, Murugadoss V, Ding T, et al. Progress on the photocatalytic reduction removal of chromium contamination. Chem Rec 2019;19(5):873–82.
[12] Nezar S, Cherifi Y, Barras A, Addad A, Dogheche E, Saoula N, et al. Efficient reduction of Cr(VI) under visible light irradiation using CuS nanostructures. Arab J Chem 2019;12(2):215–24.
[13] Du XD, Yi XH, Wang P, Zheng W, Deng J, Wang CC. Robust photocatalytic reduction of Cr(VI) on UiO-66-NH_2 (Zr/Hf) metal–organic framework membrane under sunlight irradiation. Chem Eng J 2019;356:393–9.
[14] Xia S, Song Z, Jeyakumar P, Shaheen SM, Rinklebe J, Ok YS, et al. A critical review on bioremediation technologies for Cr(VI)-contaminated soils and wastewater. Crit Rev Environ Sci Technol 2019;49(12):1027–78.
[15] Kumar V, Dwivedi SK. Hexavalent chromium reduction ability and bioremediation potential of *Aspergillus flavus* CR500 isolated from electroplating wastewater. Chemosphere 2019;237:124567.
[16] Sharma S, Malaviya P. Bioremediation of tannery wastewater by chromium resistant novel fungal consortium. Ecol Eng 2016;91:419–25.
[17] Papassiopi N, Vaxevanidou K, Christou C, Karagianni E, Antipas GS. Synthesis, characterization and stability of Cr(III) and Fe(III) hydroxides. J Hazard Mater 2014;264:490–7.
[18] Golder AK, Chanda AK, Samanta AN, Ray S. Removal of hexavalent chromium by electrochemical reduction–precipitation: investigation of process performance and reaction stoichiometry. Separ Purif Tech 2011;76(3):345–50.
[19] Chen J, Xu S, Guo S. National hazardous waste directory. J Build Mater 2016 (4):1–11. Chinese.
[20] Li C, Yu J, Li W, He Y, Qiu Y, Li P, et al. Immobilization, enrichment and recycling of Cr(VI) from wastewater using a red mud/carbon material to produce the valuable chromite ($FeCr_2O_4$). Chem Eng J 2018;350:1103–13.
[21] Erdem M, Tumen F. Chromium removal from aqueous solution by the ferrite process. J Hazard Mater 2004;109(1–3):71–7.
[22] Pei G, Wei Z, Fu H, Liu J, Yu F. Optimization of hexavalent chromium removal from wastewater by ferrite precipitation. J Residuals Sci Technol 2016;13(S2): S85–91.
[23] Song X, Wang S, Lu J. Removal of chromium and nickel ions from synthetic solution by the ferrite process. Adv Mater Res 2010;113–116:2251–4.
[24] Tu YJ, Chang CK, You CF, Wang SL. Treatment of complex heavy metal wastewater using a multi-staged ferrite process. J Hazard Mater 2012;209–210:379–84.
[25] Barrado E, Prieto F, Medina J, López FA. Characterisation of solid residues obtained on removal of Cr from waste water. J Alloys Compd 2002;335(1–2):203–9.
[26] Chang LY. Alternative chromium reduction and heavy metal precipitation methods for industrial wastewater. Environ Prog 2003;22(3):174–82.
[27] Lou JC, Huang YJ, Han JY. Treatment of printed circuit board industrial wastewater by Ferrite process combined with Fenton method. J Hazard Mater 2009;170(2–3):620–6.
[28] Ministry of Ecology and Environment of the People's Republic of China. HJ/T 299–2007: Solid waste-extraction procedure for leaching toxicity-sulphuric acid & nitric acid method. Chinese standard. Beijing: China Environmental Science Press; 2007. Chinese.
[29] Ministry of Ecology and Environment of the People's Republic of China. HJ 557–2009: Solid waste-extraction procedure for leaching toxicity-horizontal vibration method. Chinese standard. Beijing: China Environmental Science Press; 2010. Chinese.
[30] Qin L, Li Q, Wang T. Comparison of hexavalent chromium leaching efficacy of different methods from chromite ore processing residue. Inorg Chem Ind 2012;44(2):51–2. Chinese.
[31] Mandaokar SS, Dharmadhikari DM, Dara SS. Retrieval of heavy metal ions from solution via ferritisation. Environ Pollut 1994;83(3):277–82.
[32] Tamaura Y, Sasao T, Abe M, Itoh T. Ferrite formation in aqueous solution at 100–200 °C. J Colloid Interface Sci 1990;136(1):242–8.
[33] Charoenjiraphat T, Amanthigo Y. Study on heavy metal (lead, cadmium and chromium) treatment technique from artificial wastewater by ferrite process. Technical report. Bangkok: Department of Industrial Chemistry; 1997.
[34] Ministry of Ecology and Environment of the People's Republic of China. GB 8978–1996: Integrated wastewater discharge standard. Chinese standard. Beijing: China Environmental Science Press; 1998. Chinese.
[35] Perales-Pérez O, Umetsu Y. ORP-monitored magnetite formation from aqueous solutions at low temperatures. Hydrometallurgy 2000;55 (1):35–56.
[36] Blázquez G, Hernáinz F, Calero M, Martín-Lara M, Tenorio G. The effect of pH on the biosorption of Cr(III) and Cr(VI) with olive stone. Chem Eng J 2009;148 (2–3):473–9.
[37] Yun YS, Park D, Park JM, Volesky B. Biosorption of trivalent chromium on the brown seaweed biomass. Environ Sci Technol 2001;35(21):4353–8.
[38] Liang C, Liang CP, Chen CC. pH dependence of persulfate activation by EDTA/Fe(III) for degradation of trichloroethylene. J Contam Hydrol 2009;106(3–4):173–82.
[39] Lou JC, Tu YJ. Incinerating volatile organic compounds with ferrospinel catalyst $MnFe_2O_4$: an example with isopropyl alcohol. J Air Waste Manag Assoc 2005;55(12):1809–15.
[40] Martin RB. Fe^{3+} and Al^{3+} hydrolysis equilibria. Cooperativity in Al^{3+} hydrolysis reactions. J Inorg Biochem 1991;44(2):141–7.
[41] More SS, Kadam RH, Kadam AB, Shite AR, Mane DR, Jadhav KM. Cation distribution in nanocrystalline Al^{3+} and Cr^{3+} co-substituted $CoFe_2O_4$. J Alloys Compd 2010;502(2):477–9.